Journal of Engineering Physics and Thermophysics, Vol. 74, No. 4, 2001

THERMAL GRAVITATIONAL-CENTRIFUGAL CONVECTION IN A LAYER OF LIQUID HEATED FROM BELOW

V. S. Berdnikov, V. P. Zakharov, and V. A. Markov

UDC 532.5;536.25

The structure of flow and heat exchange in a horizontal, heated from below, layer of liquid whose boundaries can rotate with the same and different angular velocities have been studied numerically and experimentally. The relative role of buoyancy and centrifugal forces in the formation of the flow structure of liquids with Pr = 16 and 2700 was investigated.

In a series of works [1–3], we carried out experimental and numerical investigations of heat transfer and flow structure in horizontal layers of liquid which are enclosed between rigid boundaries that may rotate differentially and which are uniformly heated from below. This thermohydrodynamic system represents the generalization of two classical problems: the Rayleigh–Benard convection and the flow induced by a rotating disk or two disks, in the gap between them. The investigations were undertaken to elucidate the relative role of buoyancy and centrifugal forces in the formation of the flow structure and to study the relationship between the local distinctive features of the flow and local heat fluxes. Calculations and experiments were carried out for liquids with Pr = 16 (96% ethyl alcohol) and Pr = 2700 (PÉS-5 silicon–organic liquid). The geometric parameters of the problem were fixed: the height of the liquid layer H = 45 mm; the radius of the container (and of the lower boundary of the layer) R_2 = 330 mm; the radius of the upper boundary R_1 = 320 mm. In the physical experiment the initial states were as follows: a Rayleigh–Benard steady-state turbulent convection in a motionless or uniformly rotating layer [4–6]. Starting from one of these states, we experimentally investigated regimes with differential rotation of the boundaries in the range of angular velocities ±4.6 rad/sec. This system is considered, in particular, as a full-size model of a variant of the Czochralski method [2, 7], with bottom heating used for drawing large-size single crystals (of diameter of up to 600 mm) from melts. To solve the technological problems, such as the selection of an optimum range of geometrical and dynamic parameters that characterize the regimes of integral and local heat and mass exchange at the front of crystallization, information on the general properties of this type of thermohydrodynamic systems is needed.

The model is formulated for an axisymmetric case in a fixed coordinate system. The geometry of the computational domain that corresponds to the scheme of the working section of the experimental rig [1, 2] is shown in Fig. 1. Here Γ_1 is the upper cold boundary; Γ_2 is the hot lower boundary which is integral with the adiabatic side wall Γ_4; Γ_3 is the symmetry axis; Γ_5 is a portion of the free boundary of the liquid.

As a mathematical model of thermal gravitational-centrifugal convection the following equations and boundary conditions were adopted:

$$\rho_0\left[\frac{\partial V_r}{\partial t}+V_r\frac{\partial V_r}{\partial r}+V_z\frac{\partial V_r}{\partial z}\right]-\rho\frac{V_\varphi^2}{r}=$$

S. S. Kutateladze Institute of Thermophysics, Siberian Branch of the Russian Academy of Sciences, Novosibirsk, Russia; email: berdnikov@itp.nsc.ru. Translated from Inzhenerno-Fizicheskii Zhurnal, Vol. 74, No. 4, pp. 111–115, July–August, 2001. Original article submitted September 11, 2000.

1062-0125/01/7404-0992$25.00

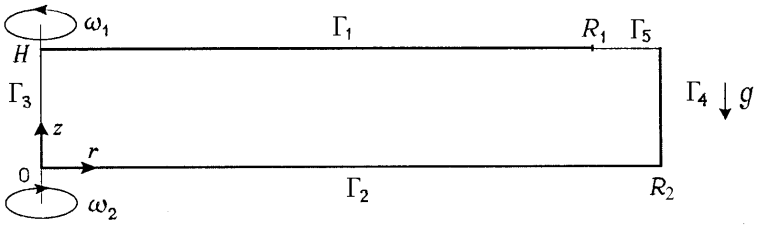

Fig. 1. Schematic diagram of the computational domain.

$$= \frac{1}{r}\left[\frac{\partial}{\partial r}\left(r\left(-p + 2\mu_0 \frac{\partial V_r}{\partial r}\right)\right) + \frac{\partial}{\partial z}\left(r\mu_0\left(\frac{\partial V_r}{\partial z} + \frac{\partial V_z}{\partial r}\right)\right) - \left(-p + 2\mu_0 \frac{V_r}{r}\right)\right];$$

$$\rho_0\left[\frac{\partial V_z}{\partial t} + V_r \frac{\partial V_z}{\partial r} + V_z \frac{\partial V_z}{\partial z}\right] = -\frac{\partial \rho}{\partial T}(T - T_0)\, g +$$

$$+ \frac{1}{r}\left[\frac{\partial}{\partial r}\left(r\mu_0\left(\frac{\partial V_z}{\partial r} + \frac{\partial V_r}{\partial z}\right)\right) + \frac{\partial}{\partial z}\left(r\left(-p + 2\mu_0 \frac{\partial V_z}{\partial z}\right)\right)\right];$$

$$\rho_0\left[\frac{\partial V_\varphi}{\partial t} + V_r \frac{\partial V_\varphi}{\partial r} + V_z \frac{\partial V_\varphi}{\partial z}\right] + \rho \frac{V_r V_\varphi}{r} =$$

$$= \frac{1}{r}\left[\frac{\partial}{\partial r}\left(r\mu_0\left(\frac{\partial V_\varphi}{\partial r} - \frac{V_\varphi}{r}\right)\right) + \frac{\partial}{\partial z}\left(r\mu_0 \frac{\partial V_\varphi}{\partial z}\right) + \mu_0\left(\frac{\partial V_\varphi}{\partial r} - \frac{V_\varphi}{r}\right)\right];$$

$$\frac{1}{r}\left[\frac{\partial}{\partial r}(r\rho_0 V_r) + \frac{\partial}{\partial z}(r\rho_0 V_z)\right] = 0;$$

$$\rho_0 C_{p0}\left[\frac{\partial T}{\partial t} + V_r \frac{\partial T}{\partial r} + V_z \frac{\partial T}{\partial z}\right] = \frac{1}{r}\left[\frac{\partial}{\partial r}\left(r\lambda_0 \frac{\partial T}{\partial r}\right) + \frac{\partial}{\partial z}\left(r\lambda_0 \frac{\partial T}{\partial z}\right)\right];$$

$$V_r\big|_{\Gamma_1} = V_r\big|_{\Gamma_2} = V_r\big|_{\Gamma_3} = V_r\big|_{\Gamma_4} = 0; \quad \mu_0 \frac{\partial V_r}{\partial z}\bigg|_{\Gamma_5} = 0;$$

$$V_z\big|_{\Gamma_1} = V_z\big|_{\Gamma_2} = 0; \quad \mu_0 \frac{\partial V_z}{\partial z}\bigg|_{\Gamma_3} = 0; \quad V_z\big|_{\Gamma_4} = V_z\big|_{\Gamma_5} = 0;$$

$$V_\varphi\big|_{\Gamma_1} = \omega_1 r; \quad V_\varphi\big|_{\Gamma_2} = \omega_2 r; \quad V_\varphi\big|_{\Gamma_3} = 0; \quad V_\varphi\big|_{\Gamma_4} = \omega_2 R_2; \quad \mu_0 \frac{\partial V_\varphi}{\partial z}\bigg|_{\Gamma_5} = 0;$$

$$T\big|_{\Gamma_1} = T_0 - \Delta T/2; \quad T\big|_{\Gamma_2} = T_0 + \Delta T/2; \quad \lambda_0 \frac{\partial T}{\partial r}\bigg|_{\Gamma_3} = \lambda_0 \frac{\partial T}{\partial r}\bigg|_{\Gamma_4} = \lambda_0 \frac{\partial T}{\partial z}\bigg|_{\Gamma_5} = 0.$$

The numerical investigations were carried out by the method of finite elements. A dimensional system of equations in the natural variables V_r, V_z, V_φ, p, and T was solved. The velocity and temperature components were expanded over the piecewise-bilinear basis, and the pressure over the piecewise-constant basis. In the evolutional algorithm the linearization and autonomization of separate equations and of their groups were performed on the basis of the Runge–Kutta scheme of the second order of accuracy. The diffusion terms were approximated following the Euler implicit scheme. The discretized equations of diffusion/convection

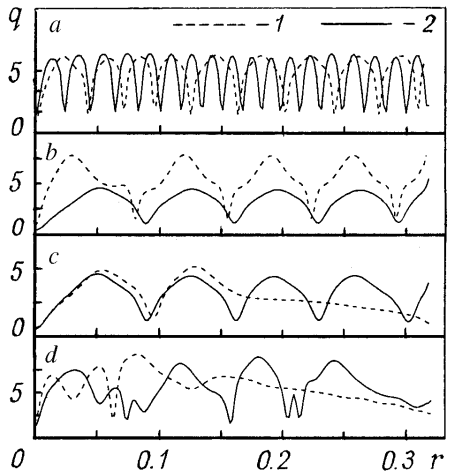

Fig. 2. Dependence of radial distributions of the local heat flux on the surface Γ_1 on the angular velocity of the rotation of the layer: a) Pr = 16; [1) ω = 2 rpm; 2) 10]; b–d) Pr = 2700; b) ω = 2 rpm; [1) Ra = 234,755; 2) 23,475]; c) Ra = 23,475; [1) ω = 80 rpm; 2) 40]; d) Ra = 234,755; [1) ω = 80 rpm; 2) 40]. *r*, mm.

were solved by the conjugate residual method. The pressure field in the calculations for Pr = 16 was sought with the aid of the SIMPLER algorithm and for Pr = 2700 with the aid of a self-sustained computational procedure. To ensure the convergence of iteration algorithms, the SLAE (systems of linear algebraic equations) scaling was applied.

With increase in the angular velocity of rotation on the whole up to 100 rpm, the evolution of an axisymmetric spatial form of convective flow of liquids with Pr = 16 and 2700 was investigated in [3]. The corresponding radial distributions of instantaneous local heat fluxes are shown in Fig. 2. The base regime of flow in the motionless layer for Pr = 16 corresponds to the value of the Rayleigh number $Ra = 6.87 \cdot 10^5$ (Fig. 2a). The effect of a decrease in the horizontal size of cellular flow with increase in ω, observed experimentally in [5, 6], was reproduced numerically at angular velocities of rotation of up to 10 rpm. This effect is most vivid at moderate values of Pr numbers. For Pr = 16 and sufficiently small values of ΔT and ω, an axisymmetric and virtually stationary cellular structure is established. The size of the cells decreases but little in the radial direction. The increase in ω leads to flow stabilization, whereas the increase in ΔT leads to an increase in the degree of nonstationarity: the structure breathes, the horizontal size of the cells undergoes a change in time, and waves of expansion and contraction of rolls run over the structure. These waves are generated near the center, where a cell of thermogravitational nature is preserved up to large values of ω. Local heat fluxes change correspondingly. The local maxima (see Fig. 2) correspond to ascending streams of the heated liquid that impinge on the upper cold boundary. At Pr = 2700 in the state of the motionless layer the convective rolls have a more clearly expressed radial inhomogeneity of their size. On imposing a weak centrifugal acceleration ($\omega \leq 10$ rpm), the size of the axial roll begins to exceed the size of the peripheral roll by approximately 20%, with the decrease in the wavelength in the radial direction being monotonic. With a further increase in the angular velocity the spatial form of flow experiences a greater and greater influence of centrifugal forces. As ω increases, the degree of inhomogeneity of the size increases, and in this case the effect of compression of cells is not observed. This effect is masked by another one: as ω increases, the size of the rolls with clockwise liquid circulation increases and the rolls with counterclockwise circulation are compressed, i.e., in the field of centrifugal forces the flow in rolls with clockwise circulation of liquid is sustained and with counterclockwise circulation is suppressed (decelerated). Finally, the cellular structure of a thermogravitational nature is suppressed, and a large-scale flow of nonisothermal liquid in the field of cen-

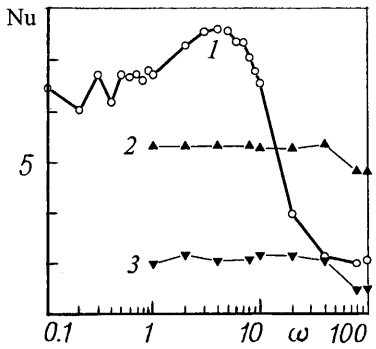

Fig. 3. Dependence of the dimensionless integral heat-transfer coefficient on the angular velocity of rotation of a liquid layer. ω, rpm.

trifugal forces originates which is similar to the flow in the vertical liquid layer in the gravity field enclosed between the walls heated to different temperatures. Correspondingly, the character of the radial distribution of local heat fluxes changes from a periodic one, typical of a cellular structure (Fig. 2a, b) to a monotonic decrease downstream typical of a laminar boundary layer (Fig. 2c, d, curves 1). The asymmetry of rolls in a convective cell is reflected on $q(r)$ (curves 2 in Fig. 2c, d). The centrifugal flow first of all occupies the periphery of the layer. An axisymmetric cell, in which a flow is formed under the gravity field, remains in the axial region.

The dependence of the integral coefficient of heat transfer (the Nusselt number $\mathrm{Nu} = q_i/(\lambda\Delta T/H)$, where $q_i = (1/\mathrm{mes}\,\Gamma_i)\int \lambda(\partial T/\partial z)d\Gamma_i$) on ω is presented in Fig. 3. When Pr = 16, a weak monotonic increase in Nu is observed with increase in ω from 0 to 5 rpm, which is due to the increase in the number of increasingly shorter laminar boundary layers on the horizontal boundaries within the limits of separate rolls. When $5 \le \omega \le 10$ rpm, a further increase in the number of rolls in the radial direction and decrease in their horizontal size leads to a decrease in the integral heat flux, since a more intense heat exchange between the ascending (hot) and descending (cold) liquid streams begins. The formation of a large-scale flow with a further increase in ω leads to the next, more substantial, decrease in the integral heat flux. Curves 2 and 3 show a similar function Nu(ω) in the case of Pr = 2700 for Ra = 234,755 and Ra = 23,475, respectively.

In the regimes of differential rotation of boundaries, starting from the state of uniform rotation of the layer as a whole, the following features and stages of development of the flow structure are observed (Fig. 4). In the state of uniform rotation at Ra = 234,755 and Pr = 2700 when $\omega_1 = \omega_2 = 10$ rpm, the flow has rather a regular cellular structure (Fig. 4a). When the speed of rotation of the upper boundary decreases, the flow becomes highly irregular in the radial direction, light deceleration (no more than by $\delta\omega_1 = -0.04$ rpm) of the upper boundary Γ_1 first causes enhancement (i.e., increase in the horizontal size) of the rolls with liquid counterclockwise circulation (Fig. 4b) and then (at $\delta\omega_1 = -0.2$ rpm) development of a large-scale centrifugal cell (Fig. 4c) with the same direction of circulation. A slight increase in the speed of rotation of Γ_1 (at $\delta\omega_1 = +0.2$ rpm) leads to the development of a centrifugal cell, but due to the enhancement of rolls with clockwise circulation. A substantial increase in ω_1 ($\delta\omega_1 = +4$ rpm) leads to the development of a large-scale forced flow (Fig. 4d; here, there is clockwise circulation of liquid) that completely suppresses the initial cellular flow. Complete stop of the upper boundary leads to the formation of a forced flow in which liquid is drawn to the rotating lower boundary in the axial region. In this case, the form of flow resembles that shown in Fig. 4d but with counterclockwise circulation of liquid. The evolution of the upper boundary in the direction opposite to the lower boundary leads to the formation of a flow with liquid drawn in the center of the layer to the upper boundary (Fig. 4e–g). In this case, a kind of competition is observed: with the motionless upper boundary the drawing of liquid in the center toward the rotating lower boundary, and then, as ω_1 in-

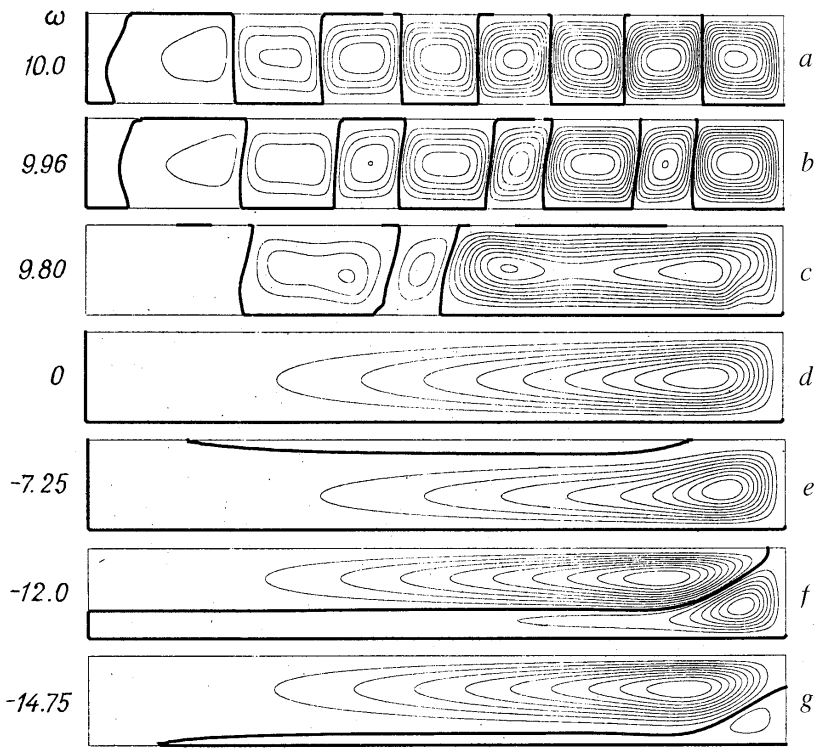

Fig. 4. Dependence of the spatial form of flow (isolines of the stream function of an axisymmetric flow) on the angular velocity of rotation of the upper boundary ω_1 for ω_2 = 10 rpm; Ra = 234,755; Pr = 2700.

creases, the drawing of liquid from the core and downward and upward to both rotating boundaries (Fig. 4f). Thereafter, complete domination of the flow is observed in which the liquid is drawn to the upper boundary, and there is a spatial shape similar to that shown in Fig. 4d. Despite the great difference in the starting conditions, this scenario of the rearrangement of flow structure agrees on a qualitative level with that observed experimentally in [1]; this first of all relates to the stages of formation of a forced large-scale flow and the corresponding changes in the integral heat flux.

The rearrangement of the structure of flow is accompanied by a change in the integral heat flux through the liquid layer (Fig. 5), the general trends of which also coincide qualitatively with those found experimentally in [1]. Figure 5 presents the values of the heat flux on the upper and lower boundaries of the layer; comparison of the data allows one to judge the heat flux balance and the accuracy of the calculations. In the regime of uniform rotation of the layer $\omega_1 = \omega_2 = 10$ rpm, Nu has a local maximum. On change in the angular velocity of the upper boundary to either side, the rearrangement of the flow structure is accompanied by a decrease in Nu. In the experiment this is caused by laminarization of a turbulent boundary layer (the portion of the small-scale cells of Rayleigh–Benard nature disappears) on a rotating surface. In the case analyzed, a similar effect is caused by a decrease in the number of cells that have dimension equal to H along the vertical. Transition from the cellular form of flow to a large-scale centrifugal convection and its intensification are accompanied by a monotonic increase in Nu with increasing ω_i. On deceleration and evolution of the upper boundary to the opposite side, the value of Nu attains a maximum value at $\omega_1 = 0$. Thereafter, a monotonic decrease in the integral heat transfer up to the attainment of the local minimum at $\omega = -7.5$ rpm is observed. The local minimum is explained by the formation of a retarded liquid layer near the upper boundary (screening of the cold boundary of the cold liquid) (Fig. 4e). The formation of the centrifugal flow near the upper boundary leads to a slight monotonic increase in Nu. The maximum value is attained in the regime when symmetric centrifugal fluxes near both boundaries are formed. A further increase in the

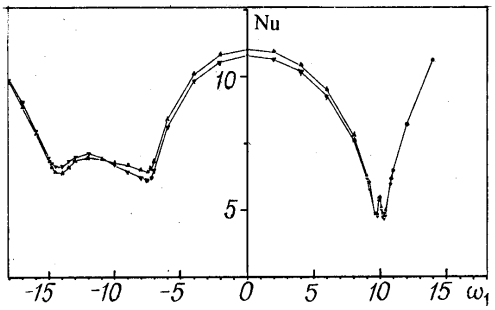

Fig. 5. Dependence of the dimensionless integral coefficient of heat transfer on the angular velocity of rotation of the upper boundary. ω_1, rpm.

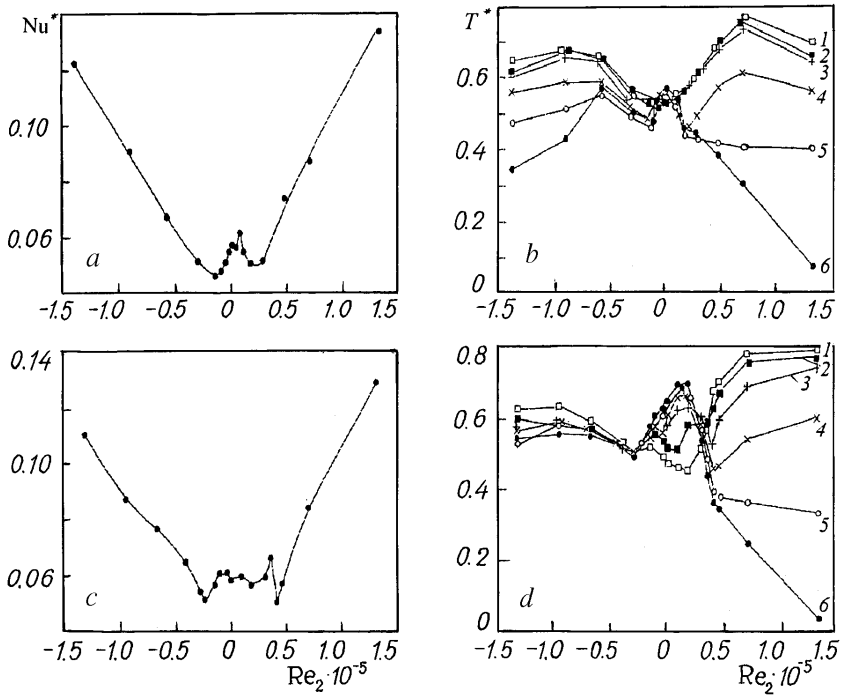

Fig. 6. Dependence of the normalized dimensionless integral heat flux (a, c) and radial distribution of the dimensionless temperature (b, d) on the angular velocity of rotation of the lower boundary.

evolution leads to suppression of the centrifugal flow near the lower boundary, screening of the heated surface by a heated liquid, and an insignificant monotonic decrease in the integral heat flux with attainment of the local minimum at $\omega = -14$ rpm. The formation of the centrigal flow with an ascending stream to the upper boundary, which almost completely suppresses the flow near the walls of the container, and its intensification with increase in ω_1 are accompanied by a monotonic increase in Nu.

Figure 6 presents experimental data on heat transfer and radial distribution of temperature that supplement the results of [1, 2]. Here $Nu^* = Nu/Ra^{1/3}$; $Nu = QH/\lambda(T_2 - T_1)$; $T_i^* = (T_i - T_1)/(T_2 - T_1)$; i is the number of thermocouples positioned at the level $z = 7$ mm from the upper boundary and at the following distances from the center of the layer: 1) $r = 2$ mm; 2) 53; 3) 103; 4) 147; 5) 200; 6) 242; a, b) $\omega_1 = 0.105$ rad/sec; c, d) $\omega_1 = 0.41$ rad/sec. The value of Ra is approximately equal to $2 \cdot 10^7$; Pr = 16 and $Re_2 = \omega_2 R_2^2/\nu$. At a fixed angular velocity of the upper boundary, the speed of rotation of the lower boundary changed smoothly. The measurements were carried out in the steady-state regime of heat exchange. The local sharp maximum on the $Nu^*(Re_2)$ curves corresponds to the regimes with $\omega_1 = \omega_2$. The process of laminarization of a boundary layer with change in the speed of rotation of one of the walls was observed through a transparent

upper boundary. In addition to direct observation of the motion of a visualized liquid, the radial stratification of the liquid by temperature serves as an indicator of the origination of a large-scale centrifugal flow. It manifests itself most vividly at large values of Re_2 (Fig. 6b, d). During the start from the state of turbulent thermogravitational convection the excitation of a global meridional flow has a threshold character and depends on the value of Ra. The excitation of this flow and its intensification with a further increase in the absolute value of Re_2 lead to a monotonic increase in heat transfer. The rearrangement of flow in transition from the regime of free convection to a forced one is rather complex. It is seen from Fig. 6a, b that at the given parameters the process of rearrangement differs insignificantly from a similar transition during the start from the state of a motionless layer ([1], Fig. 2a). The singularity as the asymmetry of the function $Nu^*(Re_2)$ is nevertheless present. The data presented in Fig. 6c, d are of interest because they show the presence of regimes with an almost constant integral heat flux in a certain range of Re_2 and simultaneously the presence, in a narrower region of parameters, of the states with the absence of radial stratification by temperature under the cold rotating surface. These regimes are of greatest interest from the technological point of view [1, 7].

Thus, we have shown numerically and experimentally that, starting from different regimes of Rayleigh–Benard convection (laminar cellular or turbulent), the superposition of the field of centrifugal forces by different means (rotation of the layer as a whole or differential rotation of boundaries) leads to certain universal stages of evolution of the flow structure and universal laws governing the change in local and integral heat exchange.

This work was carried out with financial support from the Russian Foundation of Basic Research (project code 99-01-00544) and Integration projects of the Siberian Branch of the Russian Academy of Sciences Nos. 2000-49 and 2000-55.

NOTATION

H, height of a layer of liquid; R_1, radius of the upper boundary of the layer; R_2, radius of the lower boundary of the layer; t, time; r, z, and φ, cylindrical coordinate system; ρ, density; ρ_0, density at T_0; μ_0, molecular viscosity at T_0; C_{p0}, heat capacity at T_0; λ, thermal conductivity; λ_0, thermal conductivity at T_0; ν, coefficient of kinematic viscosity; a, thermal diffusivity; q, local heat flux; g, gravity acceleration; V_r, V_z, and V_φ, radial, axial, and azimuthal velocity components; p, pressure; T, temperature; $T_0 = (T_1 + T_2)/2$; $\Delta T = T_2 - T_1$; ω, angular velocity; ω_1, angular velocity of the upper boundary; ω_2, angular velocity of the lower boundary; $\mathrm{Pr} = \nu/a$, Prandtl number; $\mathrm{Ra} = (\beta g/a\nu)\Delta T H^3$, Rayleigh number; $\mathrm{Re}_i = \omega_i R_i^2/\nu$, Reynolds number; $\mathrm{Nu} = QH/\lambda(T_2 - T_1)$, Nusselt number. Subscripts: 1, upper boundary; 2, lower boundary.

REFERENCES

1. V. S. Berdnikov and V. A. Markov, in: *"Proc. III Minsk Int. Forum "Heat and Mass Transfer–MIF-96"* [in Russian], Minsk, May 20–24, 1996 [in Russian], Vol. 1, Pt. 2, Minsk (1996), pp. 12–16.
2. V. S. Berdnikov and V. A. Markov, *Prikl. Mekh. Tekh. Fiz.*, **39**, No. 3, 126–133 (1998).
3. V. S. Berdnikov and V. P. Zakharov, in: *Dynamics of Continuum* [in Russian], Issue 114, Novosibirsk (1999), pp. 95–100.
4. V. S. Berdnikov and V. A. Markov, *Vestsi Akad. Navuk BSSR, Ser. Fiz.-Énerg. Navuk*, No. 1, 96–102 (1986).
5. H. T. Rossby, *J. Fluid Mech.*, **36**, 309–317 (1969).
6. B. M. Bubnov and G. S. Golitsyn, in: *Exercises on Turbulence* [in Russian], Moscow (1994), pp. 18–31.
7. V. I. Goriletsky, V. A. Nemenov, V. G. Protsenko, A. V. Radkevich, and L. G. Eidelman, *J. Cryst. Growth*, **52**, 509–513 (1981).